

Article

Influence of Sustainable Biochars Produced from Kitchen Waste, Pig Manure, and Wood on Soil Erosion

Xilong Huang^{1,2}, Renjie Niu^{1,2}, Xiaoli Huang^{1,2}, Yongxue An^{1,2}, Junhao Li^{1,2}, Manqi Li^{1,2}, He Huang^{1,2} and Ankit Garg^{1,2,*}

¹ Department of Civil and Environmental Engineering, Shantou University, Shantou 515063, China; 18xlhuang1@stu.edu.cn (X.H.); 18rjniu@stu.edu.cn (R.N.); 19xlhuang1@stu.edu.cn (X.H.); 19yxan@stu.edu.cn (Y.A.); 19jhli4@stu.edu.cn (J.L.); 18mqli3@stu.edu.cn (M.L.); 18hhuang2@stu.edu.cn (H.H.)
² Guangdong Engineering Center for Structure Safety and Health Monitoring, Shantou 515063, China
* Correspondence: ankit@stu.edu.cn

Abstract: The influence of biochars on water retention, mitigating nutrient leaching, and pollutant removal in green infrastructure has been explored in the past. However, there is a lack of understanding on how feedstock (i.e., biomass) would affect biochar physicochemical properties and hence, overall erosion control (including infiltration, surface, and sub-surface runoff) in green infrastructure. The main purpose of this study was to investigate the effect of biochars produced from three different feedstocks (pig manure, wood, and kitchen waste) on the erosion of granite residual soil. Flume experiments were conducted to measure and analyze soil erosion, runoff, and infiltration. The result showed that the runoff and soil erosion of kitchen waste biochar (KWB) samples were reduced by 17.7% and 21.7%, respectively. On the contrary, wood biochar (WB) and pig manure biochar (PMB) were found to enhance runoff and soil erosion. In addition, biochar particles were found in runoff and infiltration in erosion experiment. Thus, it is important to note that measures should be taken to prevent biochar loss when using biochar as a soil amendment. Additionally, the effects of different types of biochar on soil hydraulic and hydrophobicity properties should be taken into account as a selection criterion for choosing amendments in green infrastructure. This study finds that kitchen waste biochar has better performance in improving soil hydraulics and erosion.

Keywords: biochar; biochar-amended soil; flume test; soil erosion; runoff; infiltration



Citation: Huang, X.; Niu, R.; Huang, X.; An, Y.; Li, J.; Li, M.; Huang, H.; Garg, A. Influence of Sustainable Biochars Produced from Kitchen Waste, Pig Manure, and Wood on Soil Erosion. *Water* **2021**, *13*, 2296. <https://doi.org/10.3390/w13162296>

Academic Editor: Viktor O Polyakov

Received: 11 June 2021

Accepted: 18 August 2021

Published: 22 August 2021

Publisher's Note: MDPI stays neutral with regard to jurisdictional claims in published maps and institutional affiliations.



Copyright: © 2021 by the authors. Licensee MDPI, Basel, Switzerland. This article is an open access article distributed under the terms and conditions of the Creative Commons Attribution (CC BY) license (<https://creativecommons.org/licenses/by/4.0/>).

1. Introduction

Soil erosion has been a major environmental concern globally, resulting in a decline of land fertility and secondary environmental problems (e.g., environmental degradation, flooding, water pollution, etc.) [1–3]. Erosion can lead to the removal of soil and ultimately decline of vegetation and hence, the performance of green infrastructure. Quinton et al. [4] found that the mass of soil loss is about 28 billion tons per year. The rate of soil erosion in farmland is 10–40 times faster than the rate of soil formation, endangering human food security [5,6]. About 80% of agricultural land degradation is caused by soil erosion [7,8]. Moreover, soil erosion causes global warming through the loss of soil organic carbon [9,10]. More than 20% of the organic carbon produced through soil erosion turns into carbon dioxide, which not only reduces soil fertility but also aggravates the global warming effect [11]. Therefore, the control of soil erosion is necessary for restoring ecosystem services of green infrastructure.

At present, the main methods to control soil erosion are soil modification and vegetation cover. The chemical additives can improve soil aggregate and reinforce soil textile [12–15], which is considered to be an effective method to reduce soil erodibility. Chemical additives commonly used in soil amendment are fly ash [16,17], lignosulfonates [18], calcite precipitates [19], and polypropylene fibers [20]. However, the use of chemical additives for soil modification can cause leaching and is only effective for fine soils with high compactness.

Peng et al. [21] indicated that straw mulch could be a suitable material to reduce soil erosion and nutrient loss. However, the common crops cannot produce enough straw residue to be widely used [21]. Adding plant residues to the soil is an excellent measure to prevent soil degradation [22–24]. Unfortunately, the rapid decomposition of plant residues can accelerate global warming [22,25]. Vegetation cover is an effective method to control soil erosion. High-density planting, basin tillage, and sediment traps, etc., are often used to control soil erosion in agriculture [26,27]. The vegetation cover can balance the economy and environment. However, plants cannot adapt to a variety of soil conditions and engineering projects [28,29]. Therefore, it is worthwhile to consider biochar as a soil additive to improve the sustainability of vegetation cover [30].

Biochar is produced by the pyrolysis of biomass in the partial or complete absence of oxygen [31–33]. Biochar mainly comprises stable aromatic forms of organic carbon that cannot easily be returned to the atmosphere as carbon dioxide [34,35]. Therefore, biochar is thought to have a positive effect on carbon sequestration in soil. In addition to Carbon sequestration, biochar as a soil additive also can be used for soil remediation, soil amelioration, crop fertilizer, and decontamination of wastewater [36]. As an environmentally friendly product, biochar has been widely used in sewage treatment to remove toxic metals, organic pollutants, and nutrients from wastewater [37]. The application of biochar to agriculture could have a major impact on reducing global warming by reducing greenhouse gas (GHG) emissions and sequestration of atmospheric carbon [38]. Some studies investigated that the addition of biochar has a positive effect on decreasing the N and P losses via runoff [39,40]. Doan et al. [39] showed that the addition of biochar reduced the transfer of NH_4^+ and NO_3^- to water during erosion. The physicochemical properties (e.g., specific surface area, elemental composition, functional groups, etc.) of biochar vary depending on the feedstocks [41,42]. Huang et al. [43] indicated that the specific surface area of wood and kitchen waste biochar was larger than that of water hyacinth biochar. At the same time, different kinds of biochar have an influence on soil water retention [44,45]. The water retention of clay treated with crop straw biochar increased by 18.4% compared with bare clay, while wastewater sludge biochar increased the water retention by 6.8% [46]. The effects of biochar may vary with the type of feedstocks, such as agricultural waste, kitchen waste, animal manure, and so on [34]. Jun et al. [47] and Singh et al. [48] found that animal-based biochar consists mainly of animal proteins such as gelatin, collagen, and polysaccharides (cellulose, starch, and carbohydrates). However, the components of plant-based and wood-based biochar are mainly cellulose, hemicellulose, and lignin. Therefore, this study uses wood (agricultural waste), kitchen waste, and pig manure as the feedstocks of biochar. The WB, KWB, and PMB correspond to wood-based biochar, plant-based biochar (i.e., kitchen waste), and animal-based biochar (i.e., pig manure), respectively.

Since biochar significantly affects the hydraulic and mechanical properties of soil, the potential of biochar to control soil erosion has also been evaluated in literature [49–51]. The scholars studying flume experiments state that most of biochar has a positive influence on soil erosion, infiltration, and runoff [25,52,53]. Jien et al. [49] found that soil mixed with wood biochar reduced soil loss by 64% at a 5% (wt/wt) application rate. Li et al. [54] observed that the average annual runoff is reduced by 19–28%, and the average annual sediment yield is reduced by 11% after biochar treatment. Extensive studies have demonstrated the feasibility of biochar modification on erosion. Zhang et al. [55] indicated that an addition of 2% biochar enhanced the erosion of croplands, whereas trends were opposite for 5% and 8% biochar addition. Historically, erosion studies about soil–biochar composite mainly discuss the influence of biochar characteristics, such as biochar percentage [49,53] and biochar particle size [56]. There are studies that exist on studying the influence of the type of biochar on the performance of green infrastructure, including water retention [57,58], nutrient leaching mitigation [59], and pollutant removal from runoff [60]. However, few studies have documented the effects of different types of biochar on erosion, runoff, and infiltration [61,62]. Lee et al. [25] found that the biochar made from oak trees can reduce the erosion of soil by 49.8%. The biochar produced from rice straw was found to reduce erosion

of soil by 18.8% [21]. Further, biochar also enhances vegetation growth, which increases resistance to erosion. Such studies help in selecting suitable biochar as an amendment material in green infrastructure. However, the influence of different biochar types (i.e., from varying feedstocks such as animal and plant origin) on soil erosion has not been considered. Furthermore, there is a lack of interpretation of the erosion control mechanism of biochar using its physicochemical properties [39,63–66]. The novelty of this study lies in the comparison of the influence of animal- and plant-based biochars on soil erosion and its interpretation with respect to their physicochemical properties.

The main objective of this study was to assess the impacts of WB, KWB, and PMB on the erosion of granite residual soil. Flume experiments were carried out on bare soil and soil–biochar composites. Each flume experiment lasted 150 min, including 120 min of moderate rain intensity ($66.7 \text{ mm}\cdot\text{h}^{-1}$) and 30 min of heavy rain intensity ($91.7 \text{ mm}\cdot\text{h}^{-1}$). Erosion, runoff, infiltration, and water content were recorded and measured separately during rainfall simulation. Data fitting and integration were used to analyze changes in erosion, runoff, and infiltration for investigating the impact of biochar on erosion control. This study will help in the selection of appropriate biochar depending on feedstock type for usage as amendment material in green infrastructure.

2. Materials and Methods

2.1. Soil and Biochar

WB, KWB, and PMB were used in the soil erosion test. In order to analyze the microstructure of biochar, Fourier transform infrared spectroscopy (FTIR) and X-ray diffraction (XRD) analysis were carried out for various biochar. The specific surface area of biochar was determined using N adsorption isotherms at the relative pressure (P/P_0) of 0.075–1. The FTIR of biochar (Figure 1a) showed that there were abundant hydrophilic functional groups such as -OH and -COOH. In addition, biochar also has -CH₂, C=C, and -CO hydrophobic functional groups. Therefore, the hydrophilicity of different biochar varies with different raw material types. XRD analysis (Figure 1b) results showed that biochar mainly contained inorganic compounds composed of K, Na, Ca, and other elements. These elements are usually the basic mineral components of biomass. The specific surface area of biochar (Figure 1c) varies from tens to more than 100. The large specific surface area makes biochar have good adsorption capacity. The area enclosed by the curve and the x-axis is the pore volume of biochar. The pore volumes of WB, PMB, and KWB are $0.169 \text{ cm}^3\cdot\text{g}^{-1}$, $0.105 \text{ cm}^3\cdot\text{g}^{-1}$, and $0.174 \text{ cm}^3\cdot\text{g}^{-1}$, respectively.

The geotechnical characteristics of the soils used in this study are shown in Table 1. The content of coarse grain in the soil is about 40% (>2.36 mm), and the content of silt and clay is about 14%. Plastic and liquid limits of soil are 18.3% and 29.2%, respectively. The maximum dry density (MDD) and optimum moisture content (OMC) of the soil were found as $16.9 \text{ kN}\cdot\text{m}^{-3}$ and 18.8%, respectively. The soil specific surface area as measured using BET method is found to be $12.7 \text{ m}^2\cdot\text{g}^{-1}$. However, the specific surface area of KWB, PMB, and WB is $76.0 \text{ m}^2\cdot\text{g}^{-1}$, $111.5 \text{ m}^2\cdot\text{g}^{-1}$, and $66.51 \text{ m}^2\cdot\text{g}^{-1}$, respectively. Evidently, the specific surface area of biochar is more than five times that of soil. The soils can be classified as clayey sand (SC) according to ASTM D2487 [67].

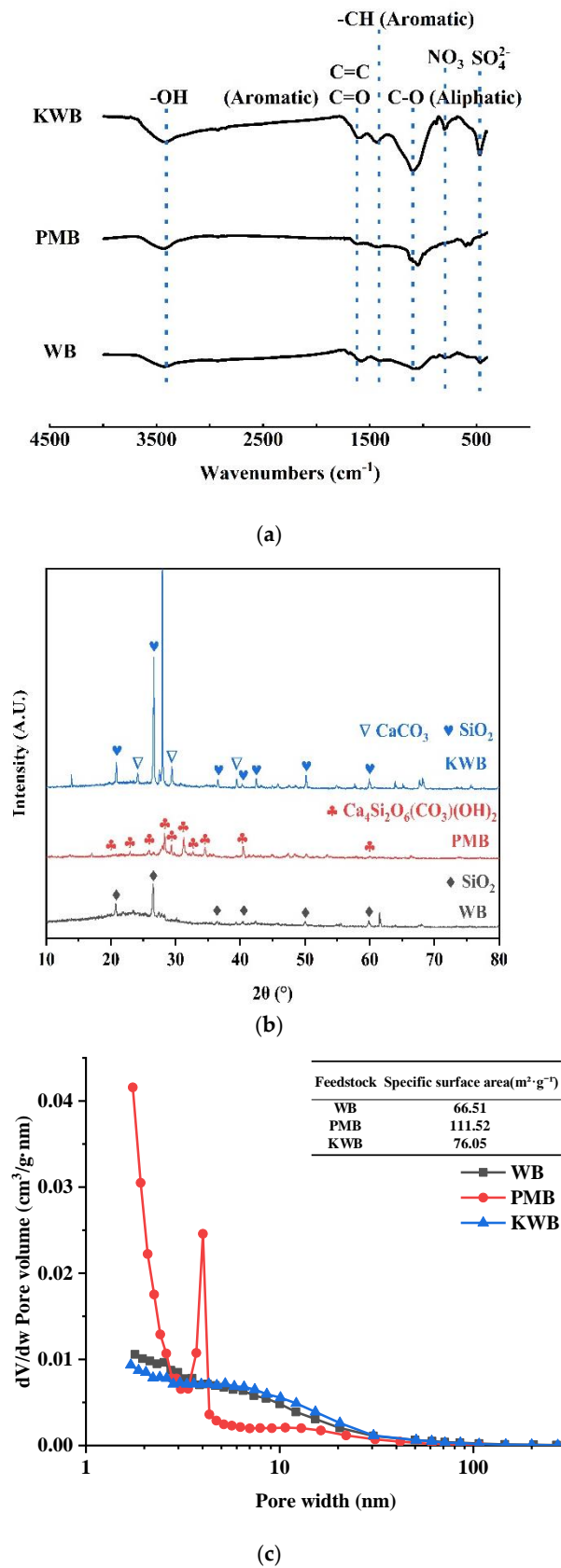


Figure 1. The microstructure of biochar: (a) FTIR analysis of biochar samples; (b) XRD analysis of biochar samples; (c) variation of pore volume with pore width obtained using BET analysis of biochar samples.

Table 1. Soil properties.

| Properties | Standard | Soil |
|--|-------------|------|
| Particle size distribution (mm) | ASTM D 422 | (%) |
| 10.0~12.5 | | 0.35 |
| 4.75~10.0 | | 12.5 |
| 2.36~4.75 | | 27.3 |
| 1.18~2.36 | | 16.7 |
| 0.60~1.18 | | 11.9 |
| 0.30~0.60 | | 7.07 |
| 0.15~0.30 | | 5.76 |
| 0.075~0.15 | | 4.32 |
| 0~0.075 | | 14.1 |
| Atterberg limits | ASTM D 4318 | |
| Liquid limit (LL/%) | | 29.2 |
| Plastic limit (PL/%) | | 18.3 |
| Plastic index (PI/%) | | 10.9 |
| MDD (kN·m ⁻³) | ASTM D 698 | 16.9 |
| OMC (%) | ASTM D 698 | 18.8 |
| Specific surface area (m ² ·g ⁻¹) | BET | 12.7 |

2.2. Soil Plot Preparation

The setup of the erosion test is shown in Figure 2. The setup was inspired by Cai et al. [68], Mhaske et al. [69], and Römkens et al. [70]. The size of the soil flume was 1.5 m in length, 1.6 m in width (0.8 m in wide for each group), and 0.2 m in height (Figure 2a). The bottom layer with 5 cm was consisted of gravels to allow infiltration into the collector. The biochar-amended soil and untreated soil were set on top of the 5-cm-thick gravel layer. Between the gravel and soil layer, a geotextile was placed to prevent any mixing of gravel and soil. To achieve a uniform density, the prepared soil–biochar mixture and the soil without biochar addition were packed uniformly into the flume in 3-cm-thick layers to a total depth of 9 cm after compaction of each layer. The prepared soil sample was placed under a rainfall simulation setup at the designed slope gradient of 7°.

2.3. Design of Rainfall Simulation

Figure 2 indicates the schematic diagram of rainfall simulator setup for flume tests. The major components of the rainfall simulator include a water supply system with spray nozzle, supporting metal frames, flow meters, collectors, and water content sensors. The rainfall simulator used in the current test was a 448-nozzle unit in design and principle of work. The water supply system was 1.5 m in length, 0.8 m in width, and 2 m above the flume. Two control valves were used to control the flow rate. The flow meters were connected to the pipe for monitoring the flow. Adopting the design of Morbidelli et al. [71], the runoff and infiltration during the rainfall event were collected separately by plastic buckets. The moisture content over time was recorded by four water content sensors (EC-5) for each group. The locations of the four sensors are shown in Figure 2b.

The input flow of the water supply system was set at 80 L·h⁻¹ and 110 L·h⁻¹, which corresponded to the rainfall intensity of 66.7 mm·h⁻¹ (low rainfall intensity) and 91.7 mm·h⁻¹ (high rainfall intensity), respectively. The relation between the input flow and rainfall intensity is as follows:

$$I = Q/A \quad (1)$$

where I is the intensity of rainfall, Q is the flow indicated by the flow meter, and A is the rainfall area. After each rainfall event, the total volume of rainfall was estimated by the following equation:

$$V_{RA} = ItA_1 \quad (2)$$

where V_{RA} is the theoretical total rainfall per unit area, I is the intensity of rainfall, t is the duration of rainfall simulation, and A_1 is the unit area (1 m²).

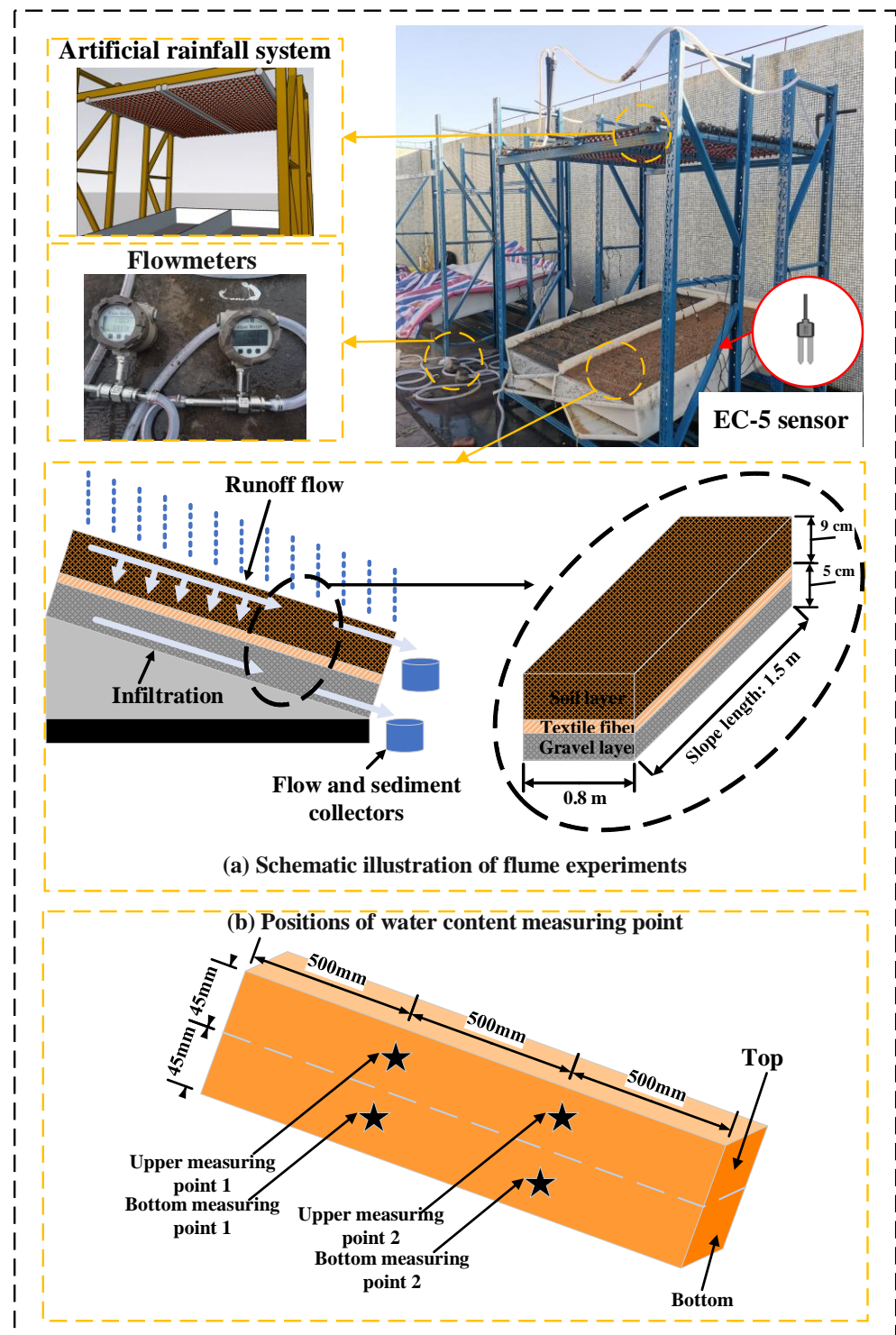


Figure 2. Setup of erosion test (a) Schematic illustration of flume experiments, (b) Positions of water content measuring point.

2.4. Rainfall Simulation

Soil samples were uniformly mixed with 5% biochar by weight. Three types of biochar, including WB, KWB, and PMB, were mixed with soil. The soil was compacted at 85% degree of compaction (DOC) on the flume by dividing the soil into three layers uniformly. Ten independent rainfall simulations were carried out in this experiment. Each rainfall

event occurred shortly after the sample had been compacted. Before each rainfall event, soil moisture content was recorded using EC-5 moisture sensor (refer to Figure 2).

For each rainfall event, the rainfall intensity was set at $66.7 \text{ mm}\cdot\text{h}^{-1}$ for 120 min at first. After 120 min, the rainfall intensity was altered immediately to $91.7 \text{ mm}\cdot\text{h}^{-1}$ for 30 min. This simulated the transition from gentle rain to heavy rain [72]. During the simulated rainfall, the erosion from the flume was collected using plastic containers. The water content was also recorded during collecting erosion. Within 10 min at the beginning of simulated rain, runoff flow, infiltration flow, and water content were recorded at 2, 5, and 10 min. Subsequently, the data of the experiment were measured every 10 min. For runoff and infiltration, only the total flow over a continuous period of 30 s was collected each time. The flow rate of runoff and infiltration could be determined from these measuring data. It should be noted that all the data need to be collected twice at the end of each rainfall event (i.e., at 120 min). After each rainfall event, the sediment collected in each sample was dried at $105 \text{ }^\circ\text{C}$ until a negligible change in mass was observed. The constant mass means the eroded mass during the rainfall event. Soil erosion rate could be determined from the measuring data. After measuring the eroded mass, sediments from the mixture of biochar and soil were kept under $1000 \text{ }^\circ\text{C}$ for 2 h to get the mass of biochar loss in soil erosion [73].

2.5. Data Analyses

The flow volume of runoff and infiltration during simulated rainfall can be deduced by integrating the flow rate with time. The formula is as follows:

$$V_t = \int Q_e dt \quad (3)$$

where V_t is the flow volume of runoff or infiltration per m^2 during a rainfall event, Q_e is the measuring flow rate per m^2 of runoff or infiltration, and t is the duration of the rainfall event. Similarly, the soil erosion during rainfall event can be deduced by integrating the soil erosion rate with time.

$$S_t = \int R_e dt \quad (4)$$

where S_t is the mass of soil erosion per m^2 during a rainfall event, R_e is the soil erosion rate per m^2 , and t is the duration of rainfall event.

One-way analysis of variance (one-way ANOVA) is a method to test the influence of different levels of the same factor on the results [74]. One-way ANOVA was used to analyze the mean values of steady flow rate and erosion rate in ten experiments. The effects of WB, PMB, and KWB on BS were evaluated.

3. Results

3.1. Variation of Runoff Rate and Infiltration Rate during Artificial Rainfall Events

As shown in Figure 3, a simplified model for the variation of runoff and infiltration rate with time is proposed. It is generally believed that the runoff and infiltration rate increase with the increase in time at the beginning of rainfall. After a certain time, the runoff and infiltration rate reach a constant value (peak). This constant value is related to rainfall intensity. According to the results shown in Figure 3a,c, the characteristic curves of runoff and infiltration rate over time under the rainfall conditions are proposed.

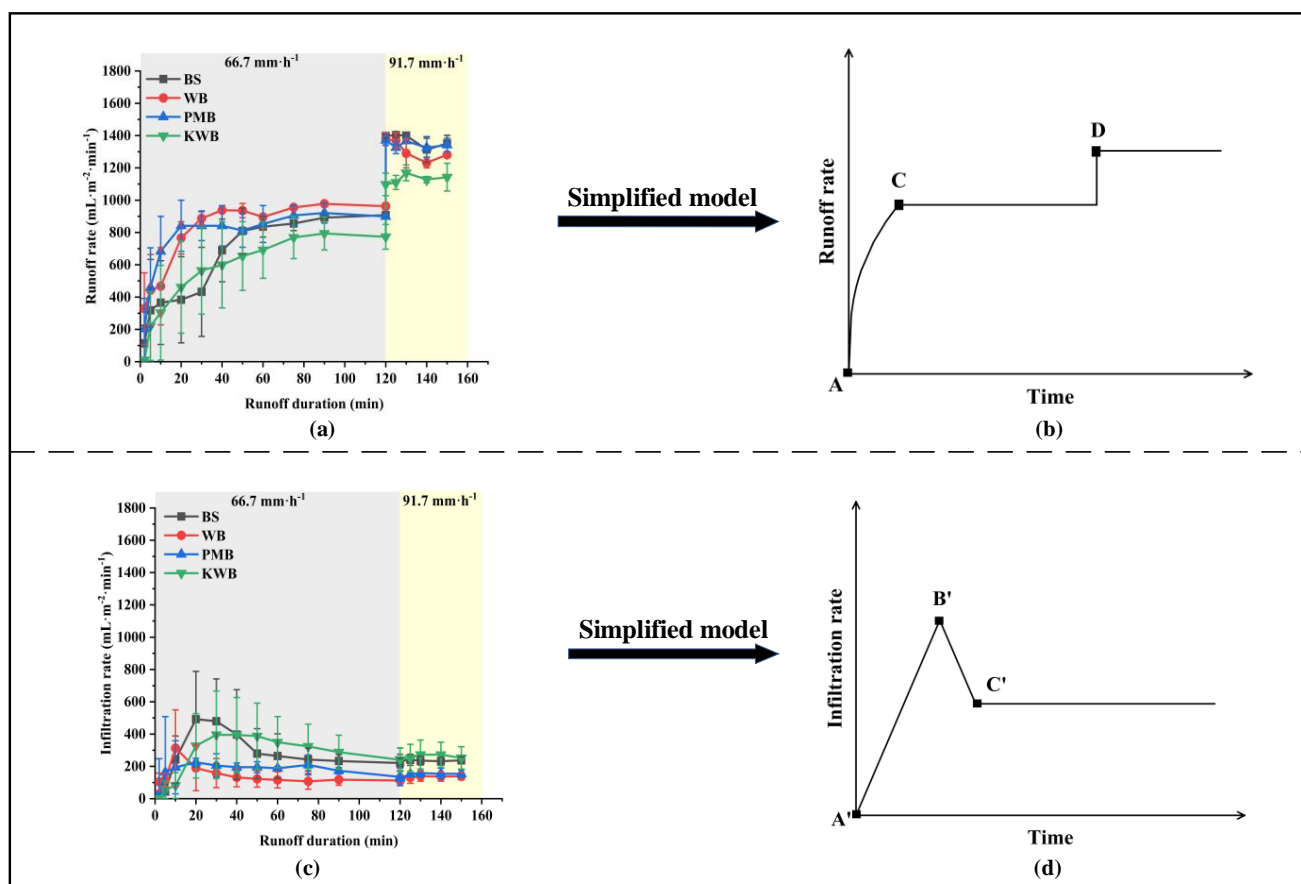


Figure 3. The flow rate (a) runoff (c) infiltration and its characteristic curve (b) runoff (d) infiltration.

The curve of runoff rate over rainfall duration is shown in Figure 3a. The event consists of 120 min of low rainfall and 30 min of heavy rainfall. At 120 min, the simulated rainfall intensity suddenly increases from $66.7 \text{ mm}\cdot\text{h}^{-1}$ to $91.7 \text{ mm}\cdot\text{h}^{-1}$. Figure 3b represents the relationship between runoff flow rate and rainfall duration. At first, the runoff flow rates of all samples increase slowly with the duration of rainfall. After about 20–40 min, the runoff flow rates increase rapidly until they reach a peak (point C). After point C, the runoff of all samples reaches a stable value. The sudden increase in rainfall intensity leads to the rapid increase in runoff flow rate. This change occurs almost simultaneously with the change in rainfall intensity. The new runoff flow rates remain stable until the rainfall ends (point D). The characteristic curve model is used to fit the data shown in Figure 3a. The fitting results are shown in Table 2, where c and d respectively represent the flow rate after the runoff and infiltration reach constant. The stable runoff flow rates of KWB are the smallest under two different rainfall intensities, which are $694.2 \text{ mL}\cdot\text{m}^{-2}\cdot\text{min}^{-1}$ and $1129.3 \text{ mL}\cdot\text{m}^{-2}\cdot\text{min}^{-1}$. The stable runoff of WB is the largest under low rainfall intensity (about $916.7 \text{ mL}\cdot\text{m}^{-2}\cdot\text{min}^{-1}$), and the stable runoff of BS is the largest under high rainfall intensity (about $1373.0 \text{ mL}\cdot\text{m}^{-2}\cdot\text{min}^{-1}$). Compared with BS, KWB effectively reduces the runoff flow by about 17%. In addition, the stable runoff of PMB, WB, and BS are very close (about 5% difference). Since the pore volume of KWB was $0.174 \text{ cm}^3\cdot\text{g}^{-1}$, which was significantly larger than that of PMB ($0.105 \text{ cm}^3\cdot\text{g}^{-1}$) and WB ($0.169 \text{ cm}^3\cdot\text{g}^{-1}$), the addition of KWB increased the pore volume of soil significantly and improved the hydraulic conductivity. Moreover, the surface hydrophilic functional groups of KWB stabilized the soil aggregates, which alleviated the surface sealing. In contrast, the surface functional groups of PMB and WB are essentially hydrophobic, creating a seal on the soil surface with very low hydraulic conductivity. The existence of the seal blocks the infiltration of rainwater, which increases the surface runoff and promotes soil erosion [53].

Table 2. Coefficients of the models fitting in rainfall events.

| | BS | WB | PMB | KWB |
|----|---------|---------|---------|---------|
| a | 0.270 | −0.012 | −0.363 | −0.016 |
| b | −1.942 | 25.657 | 37.135 | 9.368 |
| c | 845.8 | 916.7 | 787.9 | 694.2 |
| d | 1373.0 | 1310.0 | 1346.0 | 1129.3 |
| a′ | 40.948 | 49.451 | 24.493 | 21.387 |
| b′ | −2.191 | −11.617 | −1.977 | −4.067 |
| c′ | 316.839 | 620.00 | 438.410 | 779.193 |
| d′ | 262.5 | 163.6 | 190.0 | 315.0 |
| α | 59.682 | 36.346 | 30.033 | 87.039 |
| α′ | 7.345 | 10.153 | 16.562 | 30.612 |
| β′ | 24.801 | 39.286 | 125.650 | 114.137 |

$$\text{Runoff : } \begin{cases} Q_e = at^{\frac{1}{3}} + bt & (0 \ll t < \alpha) \\ Q_e = c & (\alpha \ll t \ll 120) \\ Q_e = d(t \gg 120) \end{cases} \quad \text{Infiltration : } \begin{cases} Q_e = a't & (0 \ll t < \alpha') \\ Q_e = b't + c' & (\alpha' \ll t < \beta') \\ Q_e = d' & (t \gg \beta') \end{cases}$$

where Q_e is the flow rate per m^2 of runoff or infiltration, and t is the duration of rainfall event.

The variation curve of infiltration rate with rainfall duration is shown in Figure 3c. The infiltration rate increases linearly with time until point B′. After reaching point B′, the infiltration rate decreases gradually with time until point C′. After point C′, the flow rate reaches a steady value. The characteristic curve model is used to fit the data shown in Figure 3d. The fitting results are shown in Table 2. The infiltration rates of all samples increase with the duration of rainfall until they reach a peak. After about 10–30 min, the infiltration rates decrease gradually until they stabilize. β' represent the time for the sample to reach the stability of infiltration. It takes about 125 min for the PMB sample to reach the stable infiltration state. However, BS can reach the stable infiltration state the fastest, which takes about 25 min, where D′ is the flow rate after the infiltration reaches constant. The results show that KWB has the highest stable infiltration rate (about $315.0 \text{ mL}\cdot\text{m}^{-2}\cdot\text{min}^{-1}$) and WB has the lowest stable infiltration rate (about $163.6 \text{ mL}\cdot\text{m}^{-2}\cdot\text{min}^{-1}$). Compared with BS, KWB increased the infiltration rate by about 20%, while WB significantly reduced the infiltration rate by about 38.0%. The stable infiltration rates of PMB ($190.0 \text{ mL}\cdot\text{m}^{-2}\cdot\text{min}^{-1}$) and WB are basically the same. After the sudden increase in rainfall intensity, the infiltration rates vary little. The probable reason is that prolonged rainfall has sealed the surface of the exposed soil. Surface sealing leads to a decrease in permeability and tends to be uniform.

One-way ANOVA was used to investigate the significance of different types of biochar on stable runoff and infiltration. The analysis results are shown in Table 3. It can be observed that based on the P -value, the influence of KWB on runoff is significant, and the influence of WB and PMB on infiltration is obvious. The infiltration rate of the KWB sample is the highest, and the runoff rate is the lowest. Compared with BS, KWB improved soil infiltration capacity and significantly reduces runoff. On the contrary, WB and PMB significantly inhibited soil infiltration. The effects of different biochar on slope runoff and infiltration rate are different, which may be related to the composition and surface functional groups of biochar. It can be seen from FTIR results that KWB has more hydrophilic groups than WB and PMB (e.g., -OH, C-O, NO_3 , etc.). Moreover, biochar can promote slope surface solidification due to its enhanced water retention capacity. The surface sealing of bare soil exposed to rainfall affects runoff generation by reducing permeability [75].

Table 3. ANOVA Table Resulted from Flow Rate *.

| | Source | Sum of Squares | Degree of Freedom | Mean Sum of Squares | F | P |
|-------------------|-----------------|----------------|-------------------|---------------------|--------|-------|
| Runoff rate | (1) Model | 19,845.000 | 1 | 19,845 | 4.051 | 0.059 |
| | Error | 88,187.780 | 18 | 4899.321 | | |
| | Corrected Total | 108,032.800 | 19 | | | |
| | (2) Model | 3645.000 | 1 | 3645 | 1.318 | 0.266 |
| | Error | 49,772.220 | 18 | 2765.123 | | |
| | Corrected Total | 53,417.220 | 19 | | | |
| (3) Model | 29,6867.200 | 1 | 29,6867.200 | 75.168 | 0.000 | |
| Error | 71,088.890 | 18 | 3949.383 | | | |
| Corrected Total | 36,7956.100 | 19 | | | | |
| Infiltration rate | (1) Model | 50,501.250 | 1 | 50,501.250 | 42.797 | 0.000 |
| | Error | 21,240.280 | 18 | 1180.015 | | |
| | Corrected Total | 71,741.530 | 19 | | | |
| | (2) Model | 37,411.250 | 1 | 37,411.250 | 32.521 | 0.000 |
| | Error | 20,706.940 | 18 | 1150.386 | | |
| | Corrected Total | 58,118.190 | 19 | | | |
| (3) Model | 2493.889 | 1 | 2493.889 | 0.611 | 0.445 | |
| Error | 73,473.330 | 18 | 4081.852 | | | |
| Corrected Total | 75,967.220 | 19 | | | | |

* Dependent variable: (1) WB, (2) PMB, (3) KWB.

3.2. Distribution of Total Flow Volume—Runoff, Infiltration, and Water Retention

Equation (3) is used to calculate the total volume of runoff and infiltration in the whole rainfall event. The total volumes of runoff and infiltration during the rainfall event are shown in Figure 4. Figure 4a shows the total flow volume distribution after 120 min of rainfall, that is, under the condition of low rainfall intensity. The order of the total runoff volume of each sample is $WB > PMB > BS > KWB$. The total runoff volumes of WB, PMB, BS, and KWB account for 77.2%, 74.3%, 63.2%, and 56.7% of total rainfall volume, respectively. KWB sample has the lowest total runoff volume, which is $75,626.8 \text{ mL}\cdot\text{m}^{-2}$. Compared with BS ($84,289.1 \text{ mL}\cdot\text{m}^{-2}$), KWB reduces the total runoff by 10.3%. WB and PMB increase the total runoff of the samples, which are $103,001.2 \text{ mL}\cdot\text{m}^{-2}$ and $99,093.8 \text{ mL}\cdot\text{m}^{-2}$, respectively. On the contrary, the order of the total infiltration volume of each sample is $WB < PMB < BS < KWB$. The total infiltration volumes of WB, PMB, BS, and KWB account for 12.3%, 16.3%, 25.5%, and 26.4% of the total rainfall volume, respectively. The total volume of infiltration in the KWB sample is the highest, which is $35,229.5 \text{ mL}\cdot\text{m}^{-2}$. The total infiltration volume of BS ($33,990.4 \text{ mL}\cdot\text{m}^{-2}$) is almost the same as that of KWB. Compared with BS, WB and PMB reduce the total volume of infiltration in samples, which are $16,407.5 \text{ mL}\cdot\text{m}^{-2}$ and $21,789.0 \text{ mL}\cdot\text{m}^{-2}$, respectively.

The total flow volume distribution after the rainfall lasts for 150 min is shown in Figure 4b. The order of total runoff of each sample is still $WB > PMB > BS > KWB$. At this time, however, the total runoff of WB, PMB, BS, and KWB account for 79.0%, 77.7%, 69.8%, and 61.2% of the total rainfall volume, respectively. The total infiltration volumes of WB, PMB, BS, and KWB account for 11.4%, 14.7%, 22.9%, and 24.1% of the total rainfall volume, respectively. The increase in rainfall intensity leads to the decrease in the proportion of total infiltration volume and the increase in the proportion of total runoff.

It can be observed from Figure 4 that KWB can significantly reduce the total runoff volume and increase the total infiltration volume. It can be predicted that KWB plays an active role in preventing soil erosion. However, WB and PMB lead to an increase in runoff and cause infiltration reduction. Thus, WB and PMB are not recommended to be used as soil amendment materials to prevent erosion.

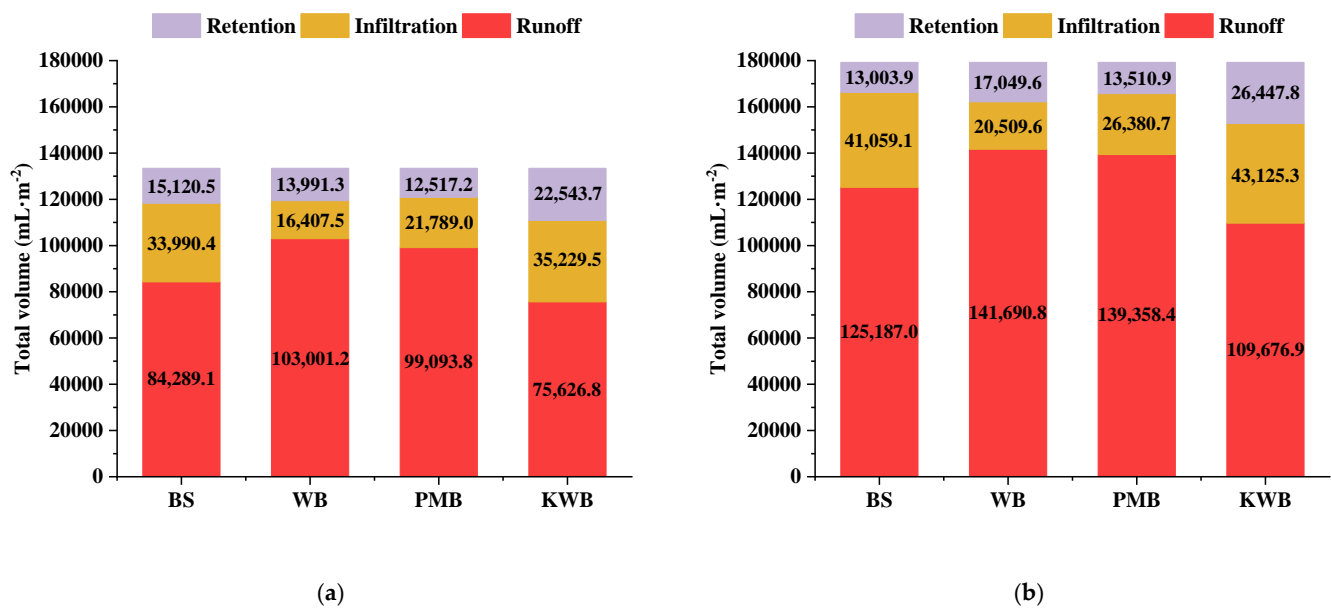


Figure 4. Total flow volume distribution during (a) 120 min of rainfall and (b) 150 min of rainfall.

The soil water balance model calculates the volume of water in soil, as reported by Littleboy et al. [76]. The relation between the rainfall volume runoff volume, infiltration volume, and water retention volume is as follows:

$$SW_i = SW_{i-1} + V_{RA} - V_{RU} - V_{SE} - V_{ET} \quad (5)$$

$$SW_i - SW_{i-1} = WR \quad (6)$$

thus,

$$WR = V_{RA} - V_{RU} - V_{SE} - V_{ET} \quad (7)$$

where SW_i is the soil water content on current time point (mL), SW_{i-1} is the soil water on previous time point (mL), V_{RA} is rainfall volume (mL), V_{ET} is evapotranspiration volume (mL), V_{RU} is runoff volume (mL), V_{SE} is infiltration volume (mL), and WR is water retention volume (mL).

Since each rainfall event lasts only 150 min, evapotranspiration can be ignored. Then, the water retention volume of samples can be calculated using Equation (7). Total flow volume distribution (runoff, infiltration, and water retention) of rainfall events at different times are summarized in Table 4. As shown in Figure 4 and Table 4, the water retention volumes of all samples are related to the runoff and infiltration. In general, high infiltration leads to a higher water retention volume. The total volume of biochar–soil amendment retained water accumulates gradually with an increase in rainfall duration. This change is also picked up by installed soil moisture sensors (see Figure 5). Figure 5 shows that the soil moisture content of most samples increases gradually with rainfall duration and then remains stable after reaching the peak. The water content increment of KWB is the largest in rainfall (from 13.4% to 25.7%). Correspondingly, its total water retention volume is also the largest (see Table 4 and Figure 4). In summary, biochar, runoff, and infiltration all affect the water retention in the soil during rainfall. The water retention of the incubated soil is reduced by the decreased infiltration rate due to surface solidification. In addition, soil internal water content and water retention are also different due to the heterogeneity of the soil medium. As shown in Figure 5, the water content captured by the upper soil moisture sensor and the bottom soil moisture sensor is often different.

Table 4. Total flow volume distribution of rainfall events at different times.

| Time (min) | Total Flow (mL·m ⁻²) | Runoff (mL·m ⁻²) | Infiltration (mL·m ⁻²) | Water Retention (mL·m ⁻²) | Time (min) | Total Flow (mL·m ⁻²) | Runoff (mL·m ⁻²) | Infiltration (mL·m ⁻²) | Water Retention (mL·m ⁻²) | | |
|------------|----------------------------------|------------------------------|------------------------------------|---------------------------------------|------------|----------------------------------|------------------------------|------------------------------------|---------------------------------------|----------|----------|
| BS | 10 | 11,116.7 | 2357.9 | 784.2 | 7974.6 | WB | 10 | 11,116.7 | 3434.6 | 1399.2 | 6283.0 |
| | 20 | 22,233.3 | 6103.7 | 4459.2 | 11,670.4 | | 20 | 22,233.3 | 9605.4 | 3911.7 | 8716.2 |
| | 30 | 33,350.0 | 10,182.8 | 9321.7 | 13,845.5 | | 30 | 33,350.0 | 17,876.3 | 5653.3 | 9820.4 |
| | 40 | 44,466.7 | 15,791.2 | 13,709.2 | 14,966.3 | | 40 | 44,466.7 | 27,001.3 | 7103.3 | 10,362.1 |
| | 60 | 66,700.0 | 31,507.9 | 19,809.2 | 15,382.9 | | 60 | 66,700.0 | 45,526.2 | 9570.0 | 11,603.8 |
| | 90 | 100,050.0 | 57,301.6 | 27,178.0 | 15,570.4 | | 90 | 100,050.0 | 73,901.2 | 12,945.0 | 13,203.8 |
| | 120 | 133,400.0 | 84,289.1 | 33,990.4 | 15,120.5 | | 120 | 133,400.0 | 103,001.2 | 16,407.5 | 13,991.3 |
| 150 | 179,250.0 | 125,187.0 | 41,059.1 | 13,003.9 | 150 | 179,250.0 | 141,690.8 | 20,509.6 | 17,049.6 | | |
| Time (min) | Total Flow (mL·m ⁻²) | Runoff (mL·m ⁻²) | Infiltration (mL·m ⁻²) | Water Retention (mL·m ⁻²) | Time (min) | Total Flow (mL·m ⁻²) | Runoff (mL·m ⁻²) | Infiltration (mL·m ⁻²) | Water Retention (mL·m ⁻²) | | |
| PMB | 10 | 11,116.7 | 3852.1 | 1185.0 | 6079.6 | KWB | 10 | 11,116.7 | 1657.9 | 425.4 | 9033.4 |
| | 20 | 22,233.3 | 11,477.1 | 3285.0 | 7471.2 | | 20 | 22,233.3 | 5482.9 | 2471.3 | 14,279.1 |
| | 30 | 33,350.0 | 198,93.8 | 5443.3 | 8012.9 | | 30 | 33,350.0 | 10,612.1 | 6087.9 | 16,650.0 |
| | 40 | 44,466.7 | 28,310.5 | 7447.4 | 8708.8 | | 40 | 44,466.7 | 16,432.9 | 10,042.1 | 17,991.7 |
| | 60 | 66,700.0 | 44,906.3 | 11,314.1 | 10,479.6 | | 60 | 66,700.0 | 29,433.0 | 17,642.1 | 19,624.9 |
| | 90 | 100,050.0 | 71,793.8 | 17,164.1 | 11,092.2 | | 90 | 100,050.0 | 52,114.3 | 27,292.1 | 20,643.6 |
| | 120 | 133,400.0 | 99,093.8 | 21,789.0 | 12,517.2 | | 120 | 133,400.0 | 75,626.8 | 35,229.5 | 22,543.7 |
| 150 | 179,250.0 | 139,358.4 | 26,380.7 | 13,510.9 | 150 | 179,250.0 | 109,676.9 | 43,125.3 | 26,447.8 | | |

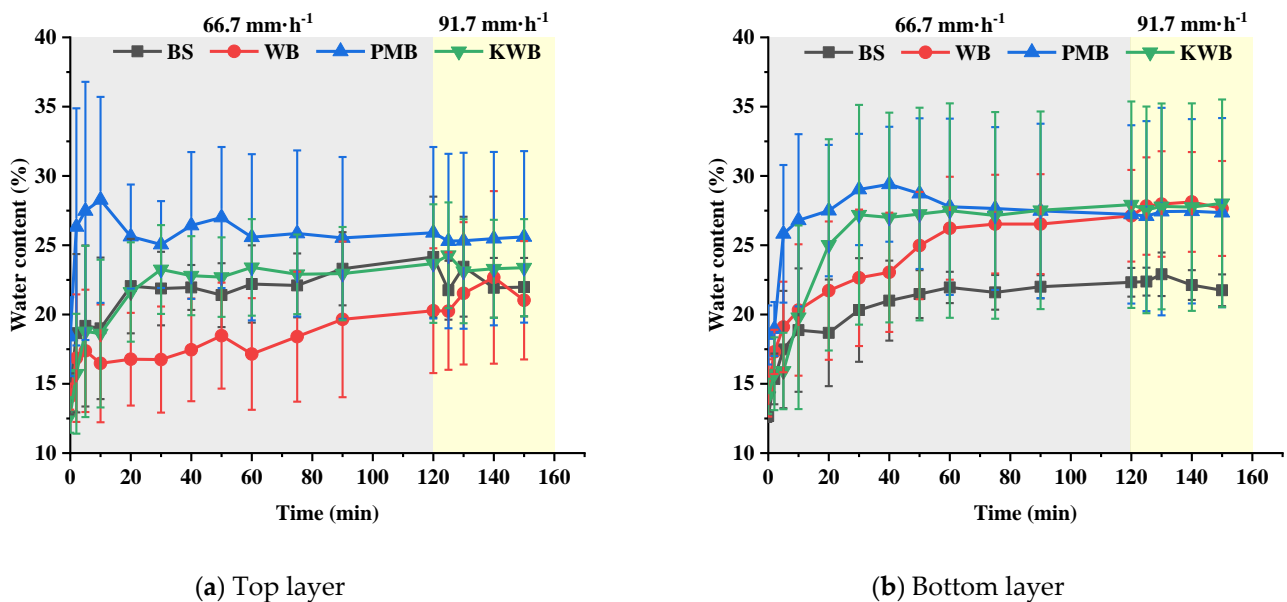


Figure 5. Variation of water content in rainfall event.

3.3. Variation of Erosion and Biochar Loss Rate

Figure 6 shows the variation of erosion rate and biochar loss rate. The event consists of 120 min of low rainfall and 30 min of heavy rainfall. At 120 min, the simulated rainfall intensity suddenly increases from 66.7 mm·h⁻¹ to 91.7mm·h⁻¹. Figure 6a represents the relationship between erosion rate in runoff and rainfall duration. At first, the erosion rates of all the samples increase with rainfall duration until they reach the peak. After about 50–60 min, the erosion rates gradually decrease until they stabilize. It takes around 90 min for the erosion rate to reach stability. KWB has the lowest peak erosion rate (about 1.75 g·m⁻²·min⁻¹). Conversely, PMB has the highest peak erosion rate (about 2.83 g·m⁻²·min⁻¹). Compared with BS, KWB effectively decreases the peak erosion rate by about 20.0%. However, PMB increases the peak erosion rate by about 30.4%. The erosion rates of all samples increase after the sudden increase of rainfall intensity. In particular, the stable erosion rate of KMB is 1.50 g·m⁻²·min⁻¹, which is the lowest of all the samples. Furthermore, the biochar loss rates of WB, PMB, and KWB account for 27.4%, 25.6%, and 24.0% of the total runoff erosion, respectively. Figure 6b represents the relationship between erosion rate in infiltration and rainfall duration. At first, the erosion rates of all the samples increase with rainfall duration until they reach the peak. After about 30–40 min, the erosion

rates gradually decrease until they stabilize. It takes around 90 minutes for the erosion rate to reach stability. The peak soil loss rates of BS, WB, PMB, and KWB are $1.08 \text{ g}\cdot\text{m}^{-2}\cdot\text{min}^{-1}$, $0.58 \text{ g}\cdot\text{m}^{-2}\cdot\text{min}^{-1}$, $2.17 \text{ g}\cdot\text{m}^{-2}\cdot\text{min}^{-1}$, and $0.75 \text{ g}\cdot\text{m}^{-2}\cdot\text{min}^{-1}$, respectively. The erosion rates of all samples increase after the sudden increase of rainfall intensity. Furthermore, the biochar loss rates of WB, PMB, and KWB account for around 44.72%, 49.87%, and 42.23% of the total infiltration erosion, respectively.

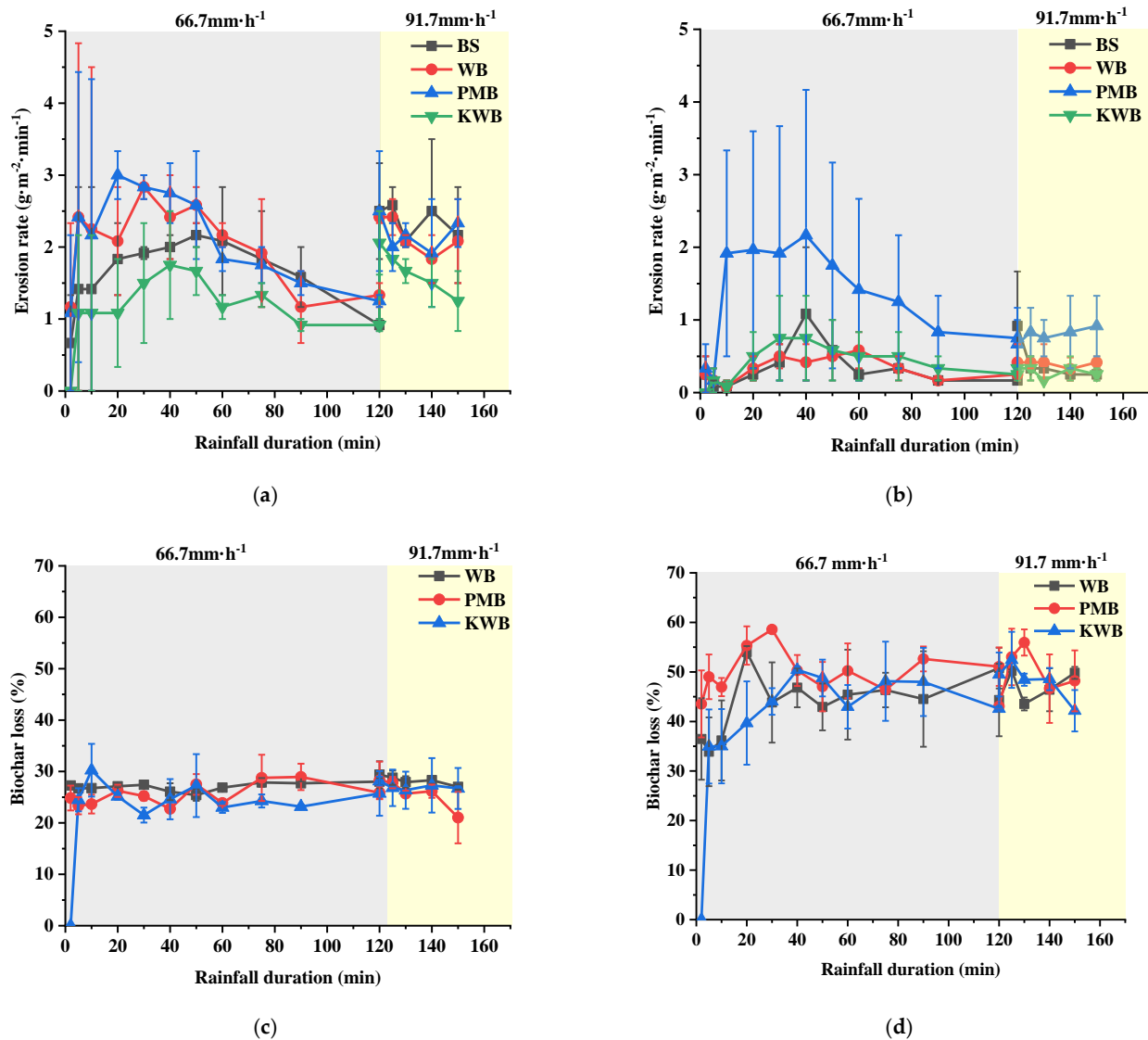


Figure 6. Effect of biochar on the erosion rate (a) runoff (b) infiltration and biochar loss (c) runoff (d) infiltration.

It can be obtained from Figures 1 and 6 that the erosion rate is related to the flow rate. A high peak flow rate leads to a high erosion rate. After the peak flow rate, sediment concentration and amplitude variation are decreased. KWB significantly reduces the runoff rate and hence the erosion rate. However, it is worth noting that the erosion rate in infiltration does not increase despite the increase in infiltration rate by KWB. On the contrary, WB and PMB enhance the runoff rate and hence the erosion rate. Nevertheless, WB and PMB also lead to an increase in erosion rate in infiltration. The results of the ANOVA are summarized in Table 5. It can be observed that based on the *P*-value, KWB has a significant impact on the erosion rate of runoff, and PMB significantly increases the erosion rate of infiltration. Thus, it is evident that KWB is a favorable amendment of soil for preventing erosion. WB and PMB, however, are not suggested to use for preventing soil erosion.

Table 5. ANOVA Table Resulted from Erosion Rate *.

| | | Source | Sum of squares | Degree of Freedom | Mean Sum of Squares | F | P |
|--------------|-----|-----------------|----------------|-------------------|---------------------|--------|-------|
| Runoff | (1) | Model | 0.200 | 1 | 0.200 | 0.612 | 0.444 |
| | | Error | 5.878 | 18 | 0.327 | | |
| | | Corrected Total | 6.078 | 19 | | | |
| | (2) | Model | 0.168 | 1 | 0.168 | 0.388 | 0.541 |
| | | Error | 7.792 | 18 | 0.433 | | |
| | | Corrected Total | 7.960 | 19 | | | |
| | (3) | Model | 2.485 | 1 | 2.485 | 7.330 | 0.014 |
| | | Error | 6.102 | 18 | 0.339 | | |
| | | Corrected Total | 8.587 | 19 | | | |
| Infiltration | (1) | Model | 0.002 | 1 | 0.002 | 0.014 | 0.908 |
| | | Error | 2.189 | 18 | 0.122 | | |
| | | Corrected Total | 2.190 | 19 | | | |
| | (2) | Model | 1.606 | 1 | 1.606 | 12.400 | 0.002 |
| | | Error | 2.331 | 18 | 0.129 | | |
| | | Corrected Total | 3.936 | 19 | | | |
| | (3) | Model | 0.089 | 1 | 0.089 | 0.793 | 0.385 |
| | | Error | 2.017 | 18 | 0.112 | | |
| | | Corrected Total | 2.106 | 19 | | | |

* Dependent variable: (1) WB (2) PMB (3) KWB.

Equation (4) is used to calculate the total erosion of runoff and infiltration in the whole rainfall event. Figure 7 shows the total erosion of samples during rainfall events. As shown in Figure 7, KWB has the lowest runoff erosion and infiltration erosion under low rainfall intensity, which are $189.5 \text{ g}\cdot\text{m}^{-2}$ and $60.5 \text{ g}\cdot\text{m}^{-2}$, respectively. Compared with BS ($270.0 \text{ g}\cdot\text{m}^{-2}$ and $49.2 \text{ g}\cdot\text{m}^{-2}$), KWB effectually reduces the runoff erosion by 29.8%. On the contrary, PMB increases runoff erosion and infiltration erosion by 12.7% and 274.8%, respectively. It is interesting that WB increases the runoff erosion of the sample but basically did not affect the infiltration erosion. It can be observed that KWB can significantly reduce the total erosion by 21.7%. On the contrary, both WB and PMB increase the total amount of erosion in the two rainfall events by 7.3% and 53.1%, respectively.

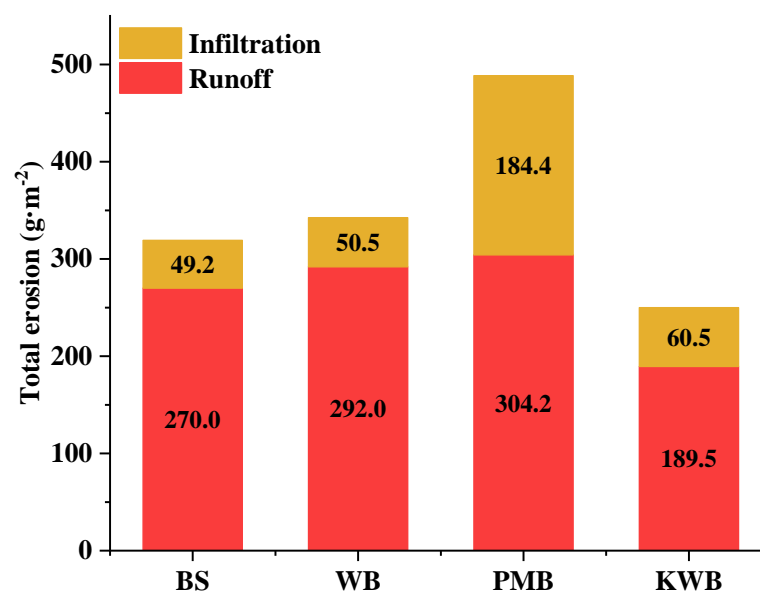


Figure 7. Total erosion in a rainfall event.

4. Discussion

The average value of repeated experiments is used to reduce the influence of error on the experimental results. It can be found that although the results of each measurement are different, the values fluctuate within the normal range. Table 6 summarizes the research results of biochar on soil erosion resistance (the biochar application rate is 5%). As shown in the table, the effect of biochar on erosion control varies with the types of biochar, the particle size of biochar, and soil properties. It can be reasonably concluded that the physical and chemical properties (i.e., shape properties and surface properties) of biochar affected by raw materials mainly determine the performance of biochar in soil. The same type of biochar has varying effects on different types of soil. In this study, 5% wood biochar enhances the erosion of sandy soil. However, as per Jien and Wang (2013) [49], 5% wood biochar can significantly reduce the erosion of highly weathered soil. In addition to the raw materials of biochar, curing time and biochar particle size also affect the effect of soil erosion resistance. However, few studies have systematically studied the effects of different types of biochar on the same type of soil. Future work should study in more detail the potential of different kinds of biochar to control the erosion of one kind of soil.

Table 6. The performance of biochar in soil erosion.

| Study | Soil | Method | Result | Remarks |
|--------------------|-----------------------|--|---|---|
| Cai et al. [68] | Colluvial soil | 5% biochar from water hyacinth | 53.7% reduction in soil erosion 32.0% decrease in runoff rate 32.5% decrease in infiltration rate | |
| Jien and wang [49] | Highly weathered soil | 5% biochar from wood | 64.0% decrease in soil erosion | |
| Zhang et al. [55] | Loam | 5% biochar from seasoned oak and hickory hardwoods | 29.5% increase in soil erosion 11.9% decrease in runoff rate 43.4% increase in soil erosion 5.6% decrease in runoff rate | Before a 140-day incubation After a 140-day incubation |
| Nyambo et al. [77] | Hutton soil | 5% biochar from maize residue | 14.2% reduction in soil erosion | |
| Li et al. [56] | Silt loam | 5% biochar from apple branches | 9.1% decrease in soil erosion 10.8% decrease in runoff rate 5.1% increase in soil erosion 8.6% decrease in runoff rate 12.5% increase in soil erosion No effect on runoff rate | The biochar particle size is 1–2 mm The biochar particle size is 0.25–1 mm The biochar particle size is less than 0.25 mm |
| Present study | Clayey sand | 5% biochar from wood | 7.3% increase in soil erosion 4.6% decrease in runoff rate | |
| | | 5% biochar from pig manure | 42.6% decrease in infiltration rate 53.1% increase in soil erosion 2.0% decrease in runoff rate | |
| | | 5% biochar from kitchen waste | 36.7% decrease in infiltration rate 21.7% decrease in soil erosion 17.7% decrease in runoff rate 9.5% decrease in infiltration rate | |

The main reason for soil erosion is the destruction of soil structure and the formation of surface seal caused by rainfall [53,78,79]. Rainfall disperses the clay on the soil surface, which further destroys soil aggregates and clogs soil pores [80]. Previous studies have shown that biochar can effectively improve soil physicochemical properties and inhibit soil erosion [49,55,68,81,82]. However, Li et al. [56] indicated that high biochar application rate and small biochar particle size have an adverse effect on soil erosion resistance. Slope gradient, slope length, soil compaction degree, and rainfall intensity also affect soil erosion resistance except for biochar [68]. This study investigated the influences of biochar type on runoff, infiltration, and erosion. The results suggested that the addition of 5% KWB could reduce the runoff and infiltration rate and restrain erosion. However, WB and PMB increased the flow rate and erosion under the same application rate. Different effects on soil erosion can be attributed to different biochar surface characteristics. The pores inside the KWB particles and pores between the biochar and soil particles can increase the soil porosity, which increases hydraulic conductivity [81–83]. Hydrophilic functional groups make soil aggregates retain water by bridging cation and soil particles under the

action of Coulomb force and van der Waals force [25]. Moreover, KWB is beneficial to the formation and stabilization of soil aggregates because it has many hydrophilic function groups (-OH, C-O, NO₃, and SO₄²⁻) on the surface [49,84]. Conversely, the FTIR indicated a clear presence of many hydrophobic functional groups in WB and PMB. The hydrophobic functional groups can break cohesive bonds formed between soil particles.

Current experiment results show that KWB inhibits soil erosion, while WB and PMB increase soil erodibility under the same conditions. The properties (e.g., surface area, function group, and pore volume, etc.) of biochar that affect water retention should be considered before its application [85]. Great care must be taken in the choice of biochar types because feedstock has a strong influence on the properties of biochar. The characteristics of biochar, such as pore volume and functional groups, affect the water and nutrients absorption capacity of biochar [83]. Biochar particles are found in runoff and infiltration in this experiment, similar to other studies [54,83]. Methods including straw covering, manure, or polyacrylamide should be taken to prevent biochar loss during rainfall [9]. In addition to soil erosion, further studies need to be conducted to assess the impact of biochar on surface runoff water quality. Further studies, particularly on biochars produced at low pyrolysis temperature, need to be conducted.

5. Conclusions

The role of biochars produced from kitchen waste, wood, and pig manure in controlling runoff and erosion is highlighted in this study. Flume experiments were conducted on bare soil and soil mixed with biochars produced from kitchen waste (KWB), wood (WB), and pig manure (PMB). One-way ANOVA revealed the influence of three types of biochar on the erosion resistance of clayey sand. The experiment results show that KWB significantly reduces the runoff and soil erosion, whereas WB and PMB have an opposite trend. It can be observed that the runoff and soil erosion of the KWB sample were reduced by 17.7% and 21.7%, respectively. Meanwhile, the addition of KWB had a significant effect on water retention (increased by 49.1%). Thus, it is evident that KWB is a favorable amendment of soil for preventing erosion. The main reasons are the highly porous structure and hydrophilic functional groups, which are abundant in KWB. In addition, biochar particles were observed in collected runoff and infiltration in this study. The biochar loss rate in runoff and infiltration erosion is around 20–30% and 40–50%, respectively. It is important to note that measures should be taken to prevent biochar loss when using biochar as a soil amendment.

This study will assist in narrowing down the selection of biochar type for its usage in green infrastructure for erosion control. Further studies are needed to study the influence of different biochar types on surface runoff and infiltration with the presence of vegetation

Author Contributions: Conceptualization, X.H. (Xilong Huang), H.H. and A.G.; methodology, X.H. (Xiaoli Huang); software, R.N., X.H. (Xilong Huang), Y.A. and M.L.; validation, X.H. (Xilong Huang), H.H. and A.G.; formal analysis, X.H. (Xilong Huang), H.H. and A.G.; investigation, X.H. (Xilong Huang), H.H. and A.G.; resources, X.H. (Xilong Huang), H.H. and A.G.; data curation, X.H. (Xiaoli Huang); writing—original draft preparation, X.H. (Xilong Huang); writing—review and editing, X.H. (Xilong Huang) and J.L.; visualization, X.H. (Xilong Huang) and H.H.; supervision, X.H. (Xilong Huang); project administration, X.H. (Xilong Huang); funding acquisition, A.G. All authors have read and agreed to the published version of the manuscript.

Funding: The research was funded by the National Natural Science Foundation of China, grant number 41907252.

Institutional Review Board Statement: Not applicable.

Informed Consent Statement: Not applicable.

Data Availability Statement: Some or all data, models, or code that support the findings of this study are available from the corresponding author upon reasonable request.

Acknowledgments: The authors would like to acknowledge the National Natural Science Foundation (NSFC) Grant (Grant number: 41907252) for the support.

Conflicts of Interest: The authors declare no conflict of interest.

References

- Morgan, R.P.C. Soil erosion: The global context. In *Soil Erosion and Conservation*, 3rd ed.; John Wiley & Sons: Malden, MA, USA, 2005.
- Morsi, R.; Bilal, M.; Iqbal, H.M.; Ashraf, S.S. Laccases and peroxidases: The smart, greener and futuristic biocatalytic tools to mitigate recalcitrant emerging pollutants. *Sci. Total Environ.* **2020**, *714*, 136572. [[CrossRef](#)]
- Borrelli, P.; Robinson, D.A.; Panagos, P.; Lugato, E.; Yang, J.E.; Alewell, C.; Wuepper, D.; Montanarella, L.; Ballabio, C. Land use and climate change impacts on global soil erosion by water (2015–2070). *Proc. Natl. Acad. Sci. USA* **2020**, *117*, 21994–22001. [[CrossRef](#)]
- Quinton, J.; Govers, G.; van Oost, K.; Bardgett, R.D. The impact of agricultural soil erosion on biogeochemical cycling. *Nat. Geosci.* **2010**, *3*, 311–314. [[CrossRef](#)]
- Stokes, A.; Douglas, G.B.; Fourcaud, T.; Giadrossich, F.; Gillies, C.; Hubble, T.; Kim, J.H.; Loades, K.W.; Mao, Z.; McIvor, I.R.; et al. Ecological mitigation of hillslope instability: Ten key issues facing researchers and practitioners. *Plant Soil* **2014**, *377*, 1–23. [[CrossRef](#)]
- Pimentel, D.; Harvey, C.; Resosudarmo, P.; Sinclair, K.; Kurz, D.; McNair, M.; Crist, S.; Shpritz, L.; Fitton, L.; Saffouri, R.; et al. Environmental and economic costs of soil erosion and conservation benefits. *Science* **1995**, *267*, 1117–1123. [[CrossRef](#)] [[PubMed](#)]
- Angima, S.; Stott, D.; O’Neill, M.; Ong, C.; Weesies, G. Soil erosion prediction using RUSLE for central Kenyan highland conditions. *Agric. Ecosyst. Environ.* **2003**, *97*, 295–308. [[CrossRef](#)]
- Comino, J.R.; Brings, C.; Lassu, T.; Iserloh, T.; Senciales, J.M.; Murillo, J.F.M.; Sinoga, J.D.R.; Seeger, M.; Ries, J.B. Rainfall and human activity impacts on soil losses and rill erosion in vineyards (Ruwer Valley, Germany). *Solid Earth* **2015**, *6*, 823–837. [[CrossRef](#)]
- Li, Z.-G.; Gu, C.-M.; Zhang, R.-H.; Ibrahim, M.; Zhang, G.-S.; Wang, L.; Chen, F.; Liu, Y. The benefic effect induced by biochar on soil erosion and nutrient loss of slopping land under natural rainfall conditions in central China. *Agric. Water Manag.* **2017**, *185*, 145–150. [[CrossRef](#)]
- Nearing, M.A.; Pruski, F.F.; O’neal, M.R. Expected climate change impacts on soil erosion rates: A review. *J. Soil Water Conserv.* **2004**, *59*, 43–50.
- da Silva, A.P.; Babujia, L.C.; Franchini, J.C.; Ralisch, R.; Hungria, M.; Guimarães, M.D.F. Soil structure and its influence on microbial biomass in different soil and crop management systems. *Soil Tillage Res.* **2014**, *142*, 42–53. [[CrossRef](#)]
- Agassi, M.; Ben-Hur, M. Stabilizing steep slopes with soil conditioners and plants. *Soil Technol.* **1992**, *5*, 249–256. [[CrossRef](#)]
- Flanagan, D.C.; Norton, L.D.; Shainberg, I. Effect of water chemistry and soil amendments on a silt loam soil—Part 1: Infiltration and runoff. *Trans. ASAE* **1997**, *40*, 1549–1554. [[CrossRef](#)]
- Jiang, H.; Cai, Y.; Liu, J. Engineering properties of soils reinforced by short discrete polypropylene fiber. *J. Mater. Civil Eng.* **2010**, *22*, 1315–1322. [[CrossRef](#)]
- Sojka, R.E.; Bjorneberg, D.L.; Entry, J.A.; Lentz, R.D.; Orts, W.J. Polyacrylamide in agriculture and environmental land management. *Adv. Agron.* **2007**, *92*, 75–162.
- Gupt, C.B.; Bordoloi, S.; Sekharan, S.; Sarmah, A.K. A feasibility study of Indian fly ash-bentonite as an alternative adsorbent composite to sand-bentonite mixes in landfill liner. *Environ. Pollut.* **2020**, *265*, 114811. [[CrossRef](#)]
- Indraratna, B.; Nutalaya, P.; Kuganenthira, N. Stabilization of a dispersive soil by blending with fly ash. *Q. J. Eng. Geol. Hydrogeol.* **1991**, *24*, 275–290. [[CrossRef](#)]
- Indraratna, B.; Muttuvel, T.; Khabbaz, H. Investigating erosional behaviour of chemically stabilised erodible soils. In *Geosustainability and Geohazard Mitigation, Proceedings of the Sessions of Geocongress 2008, New Orleans, LA, USA, 9–12 March 2008*; Reddy, K., Khire, M., Alshawabkeh, A., Eds.; Geo-Institute of The American Society of Civil Engineers: Reston, VA, USA, 2008; pp. 670–677.
- Trinh, V.N.; Tang, A.M.; Cui, Y.-J.; Dupla, J.-C.; Canou, J.; Calon, N.; Lambert, L.; Robinet, A.; Schoen, O. Mechanical characterisation of the fouled ballast in ancient railway track substructure by large-scale triaxial tests. *Soils Found.* **2012**, *52*, 511–523. [[CrossRef](#)]
- Vickers, N.J. Animal communication: When I’m calling you, will you answer too? *Curr. Biol.* **2017**, *27*, R713–R715. [[CrossRef](#)]
- Peng, X.; Zhu, Q.H.; Xie, Z.B.; Darboux, F.; Holden, N.M. The impact of manure, straw and biochar amendments on aggregation and erosion in a hillslope Ultisol. *Catena* **2016**, *138*, 30–37. [[CrossRef](#)]
- Chen, H.; Fan, M.; Billen, N.; Stahr, K.; Kuzyakov, Y. Effect of land use types on decomposition of ¹⁴C-labelled maize residue (*Zea mays* L.). *Eur. J. Soil Biol.* **2009**, *45*, 123–130. [[CrossRef](#)]
- Mikha, M.M.; Rice, C.W. Tillage and manure effects on soil and aggregate-associated carbon and nitrogen. *Soil Sci. Soc. Am. J.* **2004**, *68*, 809–816. [[CrossRef](#)]
- Sommerfeldt, T.G.; Chang, C.; Entz, T. Long-term annual manure applications increase soil organic matter and nitrogen, and decrease carbon to nitrogen ratio. *Soil Sci. Soc. Am. J.* **1988**, *52*, 1668–1672. [[CrossRef](#)]
- Lee, S.S.; Shah, H.S.; Awad, Y.; Kumar, S.; Ok, Y.S. Synergy effects of biochar and polyacrylamide on plants growth and soil erosion control. *Environ. Earth Sci.* **2015**, *74*, 2463–2473. [[CrossRef](#)]

26. Liu, X.; Zhang, S.; Zhang, X.; Ding, G.; Cruse, R. Soil erosion control practices in Northeast China: A mini-review. *Soil Tillage Res.* **2011**, *117*, 44–48. [[CrossRef](#)]
27. Posthumus, H.; Deeks, L.K.; Rickson, R.J.; Quinton, J.N. Costs and benefits of erosion control measures in the UK. *Soil Use Manag.* **2015**, *31*, 16–33. [[CrossRef](#)]
28. García-Fayos, P.; García-Ventoso, B.; Cerdà, A. Limitations to plant establishment on eroded slopes in southeastern Spain. *J. Veg. Sci.* **2000**, *11*, 77–86. [[CrossRef](#)]
29. Colesanti, C.; Wasowski, J. Investigating landslides with space-borne Synthetic Aperture Radar (SAR) interferometry. *Eng. Geol.* **2006**, *88*, 173–199. [[CrossRef](#)]
30. Prakash, A.; Bordoloi, S.; Hazra, B.; Garg, A.; Sreedeeep, S.; Zhu, H.-H. Modeling dependence among suction, moisture, and cracking of a novel biochar synthesized from weed species. *Adv. Civ. Eng. Mater.* **2020**, *9*, 90–104. [[CrossRef](#)]
31. Smith, P. Soil carbon sequestration and biochar as negative emission technologies. *Glob. Chang. Biol.* **2016**, *22*, 1315–1324. [[CrossRef](#)] [[PubMed](#)]
32. Ahmad, M.; Rajapaksha, A.U.; Lim, J.E.; Zhang, M.; Bolan, N.; Mohan, D.; Vithanage, M.; Lee, S.S.; Ok, Y.S. Biochar as a sorbent for contaminant management in soil and water: A review. *Chemosphere* **2014**, *99*, 19–33. [[CrossRef](#)]
33. Lehmann, J.; Joseph, S. (Eds.) *Biochar for Environmental Management: Science, Technology and Implementation*; Routledge: London, UK, 2015.
34. Sohi, S.P.; Krull, E.; Lopez-Capel, E.; Bol, R. A review of biochar and its use and function in soil. In *Advances in Agronomy*; Elsevier: Amsterdam, The Netherlands, 2010; Volume 105, pp. 47–82.
35. Kuhlbusch, T.A.J. Ocean chemistry: Enhanced: Black carbon and the carbon cycle. *Science* **1998**, *280*, 1903–1904. [[CrossRef](#)]
36. Wang, J.; Wang, S. Preparation, modification and environmental application of biochar: A review. *J. Clean. Prod.* **2019**, *227*, 1002–1022. [[CrossRef](#)]
37. Xiang, W.; Zhang, X.; Chen, J.; Zou, W.; He, F.; Hu, X.; Tsang, D.; Ok, Y.S.; Gao, B. Biochar technology in wastewater treatment: A critical review. *Chemosphere* **2020**, *252*, 126539. [[CrossRef](#)] [[PubMed](#)]
38. Qambrani, N.A.; Rahman, M.; Won, S.; Shim, S.; Ra, C. Biochar properties and eco-friendly applications for climate change mitigation, waste management, and wastewater treatment: A review. *Renew. Sustain. Energy Rev.* **2017**, *79*, 255–273. [[CrossRef](#)]
39. Doan, T.T.; Henry-Des-Tureaux, T.; Rumpel, C.; Janeau, J.-L.; Jouquet, P. Impact of compost, vermicompost and biochar on soil fertility, maize yield and soil erosion in Northern Vietnam: A three year mesocosm experiment. *Sci. Total Environ.* **2015**, *514*, 147–154. [[CrossRef](#)]
40. Lee, C.-H.; Wang, C.-C.; Lin, H.-H.; Lee, S.S.; Tsang, D.; Jien, S.-H.; Ok, Y.S. In-situ biochar application conserves nutrients while simultaneously mitigating runoff and erosion of an Fe-oxide-enriched tropical soil. *Sci. Total Environ.* **2018**, *619*, 665–671. [[CrossRef](#)]
41. Zhao, L.; Cao, X.; Mašek, O.; Zimmerman, A. Heterogeneity of biochar properties as a function of feedstock sources and production temperatures. *J. Hazard. Mater.* **2013**, *256–257*, 1–9. [[CrossRef](#)]
42. Kloss, S.; Zehetner, F.; Dellantonio, A.; Hamid, R.; Ottner, F.; Liedtke, V.; Schwanninger, M.; Gerzabek, M.; Soja, G. Characterization of slow pyrolysis biochars: Effects of feedstocks and pyrolysis temperature on biochar properties. *J. Environ. Qual.* **2012**, *41*, 990–1000. [[CrossRef](#)]
43. Huang, H.; Reddy, N.G.; Huang, X.; Chen, P.; Wang, P.; Zhang, Y.; Huang, Y.; Lin, P.; Garg, A. Effects of pyrolysis temperature, feedstock type and compaction on water retention of biochar amended soil. *Sci. Rep.* **2021**, *11*, 1–19. [[CrossRef](#)]
44. Hussain, R.; Ravi, K.; Garg, A. Influence of biochar on the soil water retention characteristics (SWRC): Potential application in geotechnical engineering structures. *Soil Tillage Res.* **2020**, *204*, 104713. [[CrossRef](#)]
45. Wang, D.; Li, C.; Parikh, S.J.; Scow, K.M. Impact of biochar on water retention of two agricultural soils—A multi-scale analysis. *Geoderma* **2019**, *340*, 185–191. [[CrossRef](#)]
46. Sun, F.; Lu, S. Biochars improve aggregate stability, water retention, and pore-space properties of clayey soil. *J. Plant Nutr. Soil Sci.* **2013**, *177*, 26–33. [[CrossRef](#)]
47. Jung, J.-M.; Oh, J.-I.; Baek, K.; Lee, J.; Kwon, E.E. Biodiesel production from waste cooking oil using biochar derived from chicken manure as a porous media and catalyst. *Energy Convers. Manag.* **2018**, *165*, 628–633. [[CrossRef](#)]
48. Singh, B.; Singh, B.P.; Cowie, A.L. Characterisation and evaluation of biochars for their application as a soil amendment. *Soil Res.* **2010**, *48*, 516–525. [[CrossRef](#)]
49. Jien, S.-H.; Wang, C.-S. Effects of biochar on soil properties and erosion potential in a highly weathered soil. *Catena* **2013**, *110*, 225–233. [[CrossRef](#)]
50. Basso, A.S.; Miguez, F.E.; Laird, D.A.; Horton, R.; Westgate, M. Assessing potential of biochar for increasing water-holding capacity of sandy soils. *GCB Bioenergy* **2012**, *5*, 132–143. [[CrossRef](#)]
51. Gholami, L.; Karimi, N.; Kaviani, A. Soil and water conservation using biochar and various soil moisture in laboratory conditions. *Catena* **2019**, *182*, 104151. [[CrossRef](#)]
52. Rees, G.N.; Baldwin, D.S.; Watson, G.O.; Hall, K.C. Sulfide formation in freshwater sediments, by sulfate-reducing microorganisms with diverse tolerance to salt. *Sci. Total Environ.* **2010**, *409*, 134–139. [[CrossRef](#)]
53. Abrol, V.; Ben-Hur, M.; Verheijen, F.; Keizer, J.J.; Martins, M.; Tenaw, H.; Tchekansky, L.; Graber, E.R. Biochar effects on soil water infiltration and erosion under seal formation conditions: Rainfall simulation experiment. *J. Soils Sediments* **2016**, *16*, 2709–2719. [[CrossRef](#)]

54. Li, Z.; Liu, C.; Dong, Y.; Chang, X.; Nie, X.; Liu, L.; Xiao, H.; Lu, Y.; Zeng, G. Response of soil organic carbon and nitrogen stocks to soil erosion and land use types in the Loess hilly-gully region of China. *Soil Tillage Res.* **2017**, *166*, 1–9. [[CrossRef](#)]
55. Zhang, F.; Huang, C.; Yang, M.; Zhang, J.; Shi, W. Rainfall simulation experiments indicate that biochar addition enhances erosion of loess-derived soils. *Land Degrad. Dev.* **2019**, *30*, 2272–2286. [[CrossRef](#)]
56. Li, Y.; Zhang, F.; Yang, M.; Zhang, J. Effects of adding biochar of different particle sizes on hydro-erosional processes in small scale laboratory rainfall experiments on cultivated loessial soil. *Catena* **2018**, *173*, 226–233. [[CrossRef](#)]
57. Wang, H.; Zhang, K.; Gan, L.; Liu, J.; Mei, G. Expansive soil-biochar-root-water-bacteria interaction: Investigation on crack development, water management and plant growth in green infrastructure. *Int. J. Damage Mech.* **2021**, *30*, 595–617. [[CrossRef](#)]
58. Kumar, H.; Huang, S.; Mei, G.; Garg, A. Influence of feedstock type and particle size on efficiency of biochar in improving tensile crack resistance and shear strength in lean clayey soil. *Int. J. Damage Mech.* **2021**, *30*, 646–661. [[CrossRef](#)]
59. Kuoppamäki, K.; Lehvävirta, S. Mitigating nutrient leaching from green roofs with biochar. *Landsc. Urban Plan.* **2016**, *152*, 39–48. [[CrossRef](#)]
60. Kuoppamäki, K.; Hagner, M.; Valtanen, M.; Setälä, H. Using biochar to purify runoff in road verges of urbanised watersheds: A large-scale field lysimeter study. *Watershed Ecol. Environ.* **2019**, *1*, 15–25. [[CrossRef](#)]
61. Xie, T.; Reddy, K.R.; Wang, C.; Yargicoglu, E.; Spokas, K. Characteristics and applications of biochar for environmental remediation: A review. *Crit. Rev. Environ. Sci. Technol.* **2015**, *45*, 939–969. [[CrossRef](#)]
62. Bordoloi, S.; Gadi, V.K.; Hussain, R.; Sahoo, L.; Garg, A.; Sreedeeep, S.; Mei, G.; Poulsen, T.G. Influence of *Eichhornia crassipes* fibre on water retention and cracking of vegetated soils. *Géotechnique Lett.* **2018**, *8*, 130–137. [[CrossRef](#)]
63. Ahmadi, S.H.; Ghasemi, H.; Sepaskhah, A.R. Rice husk biochar influences runoff features, soil loss, and hydrological behavior of a loamy soil in a series of successive simulated rainfall events. *Catena* **2020**, *192*, 104587. [[CrossRef](#)]
64. Kushwaha, D.P.; Kumar, A.; Chaturvedi, S. Determining the effectiveness of carbon-based stabilizers blends in arresting soil erosion and elevating properties of Mollisols soils of North Western Himalayas. *Environ. Technol. Innov.* **2021**, *23*, 101768. [[CrossRef](#)]
65. Sadeghi, S.H.; Kiani-Harchegani, M.; Hazbavi, Z.; Sadeghi, P.; Angulo-Jaramillo, R.; Lassabatere, L.; Younesi, H. Field measurement of effects of individual and combined application of biochar and polyacrylamide on erosion variables in loess and marl soils. *Sci. Total Environ.* **2020**, *728*, 138866. [[CrossRef](#)]
66. Shen, Z.; Zhang, Z.; Zhang, M.; Rinklebe, J.; Ma, Y.; Hou, D. Effect of production temperature and particle size of rice husk biochar on mercury immobilization and erosion prevention of a mercury contaminated soil. *J. Hazard. Mater.* **2021**, *420*, 126646. [[CrossRef](#)]
67. ASTM Committee D-18 on Soil and Rock. In *Standard Practice for Classification of Soils for Engineering Purposes (Unified Soil Classification System) 1*; ASTM International: West Conshohocken, PA, USA, 2017.
68. Cai, W.; Huang, H.; Chen, P.; Huang, X.; Gaurav, S.; Pan, Z.; Lin, P. Effects of biochar from invasive weed on soil erosion under varying compaction and slope conditions: Comprehensive study using flume experiments. *Biomass Convers. Biorefinery* **2020**, 1–20. [[CrossRef](#)]
69. Mhaske, S.N.; Pathak, K.; Basak, A. A comprehensive design of rainfall simulator for the assessment of soil erosion in the laboratory. *Catena* **2019**, *172*, 408–420. [[CrossRef](#)]
70. Römkens, M.; Helming, K.; Prasad, S. Soil erosion under different rainfall intensities, surface roughness, and soil water regimes. *Catena* **2002**, *46*, 103–123. [[CrossRef](#)]
71. Morbidelli, R.; Corradini, C.; Saltalippi, C.; Flammini, A.; Dari, J.; Govindaraju, R.S. A new conceptual model for slope-infiltration. *Water* **2019**, *11*, 678. [[CrossRef](#)]
72. Dunkerley, D. Effects of rainfall intensity fluctuations on infiltration and runoff: Rainfall simulation on dryland soils, Fowlers Gap, Australia. *Hydrol. Process.* **2012**, *26*, 2211–2224. [[CrossRef](#)]
73. Wang, C.; Walter, M.; Parlange, J.-Y. Modeling simple experiments of biochar erosion from soil. *J. Hydrol.* **2013**, *499*, 140–145. [[CrossRef](#)]
74. Kim, T.K. Understanding one-way ANOVA using conceptual figures. *Korean J. Anesthesiol.* **2017**, *70*, 22–26. [[CrossRef](#)]
75. Morin, J.; Benyamini, Y. Rainfall infiltration into bare soils. *Water Resour. Res.* **1977**, *13*, 813–817. [[CrossRef](#)]
76. Littleboy, M.; Silburn, D.M.; Freebairn, D.M.; Woodruff, D.R.; Hammer, G.L.; Leslie, J.K. Impact of soil erosion on production in cropping systems. I. Development and validation of a simulation model. *Soil Res.* **1992**, *30*, 757–774. [[CrossRef](#)]
77. Nyambo, P.; Taeni, T.; Chiduzza, C.; Araya, T. Effects of maize residue biochar amendments on soil properties and soil loss on acidic Hutton soil. *Agronomy* **2018**, *8*, 256. [[CrossRef](#)]
78. Assouline, S.; Mualem, Y. Modeling the dynamics of seal formation and its effect on infiltration as related to soil and rainfall characteristics. *Water Resour. Res.* **1997**, *33*, 1527–1536. [[CrossRef](#)]
79. Assouline, S.; Ben-Hur, M. Effects of rainfall intensity and slope gradient on the dynamics of interrill erosion during soil surface sealing. *Catena* **2006**, *66*, 211–220. [[CrossRef](#)]
80. Lado, M.; Paz, A.; Ben-Hur, M. Organic matter and aggregate size interactions in infiltration, seal formation, and soil loss. *Soil Sci. Soc. Am. J.* **2004**, *68*, 935–942. [[CrossRef](#)]
81. Masiello, C.A.; Dugan, B.; Brewer, C.E.; Spokas, K.A.; Novak, J.M.; Liu, Z.; Sorrenti, G. Biochar effects on soil hydrology. In *Biochar for Environmental Management*; Lehmann, J., Joseph, S., Eds.; Routledge: Abingdon, UK; New York, NY, USA, 2015; pp. 575–594.

-
82. Herath, H.; Arbestain, M.C.; Hedley, M. Effect of biochar on soil physical properties in two contrasting soils: An Alfisol and an Andisol. *Geoderma* **2013**, *209*, 188–197. [[CrossRef](#)]
 83. Sadeghi, S.H.; Hazbavi, Z.; Harchegani, M.K. Controllability of runoff and soil loss from small plots treated by vinasse-produced biochar. *Sci. Total Environ.* **2016**, *541*, 483–490. [[CrossRef](#)]
 84. Brodowski, S.; John, B.; Flessa, H.; Amelung, W. Aggregate-occluded black carbon in soil. *Eur. J. Soil Sci.* **2006**, *57*, 539–546. [[CrossRef](#)]
 85. Mao, J.; Zhang, K.; Chen, B. Linking hydrophobicity of biochar to the water repellency and water holding capacity of biochar-amended soil. *Environ. Pollut.* **2019**, *253*, 779–789. [[CrossRef](#)]